




Cite this: *RSC Adv.*, 2021, 11, 27193

# Metal-centered monocyclic carbon wheel clusters with record coordination numbers in planar species†

Xiao-Qin Lu, Hai-Gang Lu \* and Si-Dian Li \*

The highest coordination number identified to date in planar species is CN = 10 in metal-centered monocyclic boron wheel clusters  $D_{10h}$   $M@B_{10}^-$  ( $M = Ta$  and  $Nb$ ) (Galeev *et al.*, *Angew. Chem. Int. Ed.*, 2012, 51, 2101). Extensive global minimum searches and first-principles theory calculations performed herein indicate that the experimentally observed  $LaC_{13}^+$  and  $LaC_{14}^+$  possess the well-defined global minima of perfect metal-centered monocyclic carbon wheel  $D_{13h}$   $La@C_{13}^+$  (1) ( $1A_1'$ ) and slightly off-centered  $C_{2v}$   $La@C_{14}^+$  (4) ( $1A_1$ ) with record coordination numbers of CN = 13 and 11 in planar structures, respectively, further pushing the boundary of our understanding of chemical structures and bonding. Detailed molecular orbital, nucleus-independent chemical shift, and ring current analyses indicate that  $D_{13h}$   $La@C_{13}^+$  (1) is  $\sigma + \pi$  dually aromatic in nature, with 14 totally delocalized in-plane  $\sigma$  electrons and 14 totally delocalized out-of-plane  $\pi$  electrons each matching the  $4N + 2$  aromatic rule ( $N_\sigma = N_\pi = 3$ ). Similar  $\sigma + \pi$  dually aromatic metal-centered monocyclic wheel clusters  $D_{13h}$   $Ca@C_{13}$  (2),  $C_{13v}$   $Ac@C_{13}^+$  (3),  $C_{2v}$   $Y@B_6C_6^+$  (5), and  $C_{2v}$   $Sc@B_5C_6$  (6) have also been obtained with CN = 13, 13, 12, and 11, respectively. The results obtained in this work effectively enrich the chemical structures and bonding patterns of planar hypercoordinated complexes.

Received 12th July 2021  
Accepted 3rd August 2021

DOI: 10.1039/d1ra05367a

rsc.li/rsc-advances

## 1. Introduction

Searching for the maximum coordination number in planar species has fascinated chemists for many years and continuously pushed the boundary of our understanding of chemical structures and bonding.<sup>1,2</sup> The central atom and periphery atoms around it in the ligand in stable planar hypercoordinated structures must match both geometrically and electronically, *i.e.*, they must have the right atomic sizes and electronic configurations. The experimentally observed boron-centered monocyclic boron wheel clusters  $D_{7h}$   $B@B_7^{2-}$  and  $D_{8h}$   $B@B_8^-$  are good examples in which the central B atoms have the coordination numbers of CN = 7 and 8, respectively.<sup>3</sup> These boron cluster monoanions prove to be  $\sigma + \pi$  dually aromatic in nature with six delocalized  $\sigma$  and six delocalized  $\pi$  electrons ( $6\sigma + 6\pi$ ) each conforming to the  $4N + 2$  aromatic rule ( $N_\sigma = N_\pi = 1$ ). Based on the double aromaticity requirement in bare boron wheel clusters, a general electronic design principle  $x + n + k = 12$  or  $16$  was developed for metal-centered monocyclic boron wheel clusters  $M@B_n^{k-}$  by the groups of Wang and Boldyrev,<sup>1,4-6</sup> where  $x$  stands for the formal valence of the metal center  $M$ . This design principle has been successfully applied to the

experimentally characterized octacoordinated  $D_{8h}$   $Co@B_8^-$  with CN = 8,<sup>5</sup> nonacoordinated  $D_{9h}$   $Ru@B_9^-$ ,  $D_{9h}$   $Rh@B_9^-$ , and  $D_{9h}$   $Ir@B_9^-$  with CN = 9,<sup>7,8</sup> and, finally, to the decacoordinated  $D_{10h}$   $Ta@B_{10}^-$  and  $D_{10h}$   $Nb@B_{10}^-$  with CN = 10 which has proven to be the highest coordination number in planar species observed to date.<sup>1,2</sup>

However, planar hypercoordination chemistry may go well beyond metal-centered monocyclic boron wheel clusters. The recent experimental characterization of perfect planar  $D_{9h}$   $C_{18}$  by atom manipulations and high-resolution atomic force microscopy<sup>9</sup> inspires us to coordinate transition metal centers with bare cyclo[ $n$ ]carbon ring-like clusters ( $C_n$ ,  $n \geq 11$ ) to form metal-centered monocyclic carbon wheel complexes  $M@C_n^{k+}$ . Very recently, the electronic properties of metal-carbon ring complexes such as  $Li@C_{18}$  and  $MC_{16}$  have been reported.<sup>10,11</sup> Carbon ( $[He]2s^22p^2$ ) is known to be effective ligand to various transition metals with a smaller covalent radius than boron ( $[He]2s^22p^1$ ), while group IIIB metals La, Y, and Sc with the valence electronic configurations of  $(n-1)d^1ns^2$  possess the largest covalent radii in the periodic table.<sup>12</sup> Metal-centered monocyclic carbon wheel clusters  $M@C_n^{k+}$  ( $M = La, Y, Sc$ ) are thus possible to have even higher coordination numbers than their boron counterparts  $M@B_n^{k-}$ . In fact, two families of  $LaC_n^+$  monocations ( $n = 12-40$ ) were observed in mobility measurements as early as in 1994, with a La atom inserted into the carbon ring for even-numbered clusters or attached to the inside or outside of the carbon ring for odd-numbered

Nanocluster Laboratory, Institute of Molecular Science, Shanxi University, Taiyuan 030006, China. E-mail: luhg@sxu.edu.cn; lisidian@sxu.edu.cn

† Electronic supplementary information (ESI) available. See DOI: 10.1039/d1ra05367a



clusters.<sup>13</sup> More detailed mass spectra were reported late on  $\text{LaC}_n^+$  in which  $\text{LaC}_{13}^+$  appeared to be a prominent species with the La center most likely attached inside a  $\text{C}_{13}$  ring (ring Ib), while  $\text{LaC}_{14}^+$  was the only  $\text{LaC}_{2n}^+$  cluster with even number of C atoms for which ring Ib structure had a higher mass intensity than its competing isomer with a La atom inserted into a  $\text{C}_{14}$  ring (ring Ia).<sup>14</sup> Similar prominent mass peaks were also observed for  $\text{YC}_{13}^+$ ,  $\text{CeC}_{13}^+$ , and  $\text{ScC}_{13}^+$ .<sup>15</sup> Early density functional theory (DFT) calculations indicated that the most stable isomer of  $\text{LaC}_{13}^+$  possessed a nearly-cumulenenic structure with the La atom located at the center of the carbon ring.<sup>16,17</sup> However, the unique role these experimentally observed  $\text{LaC}_n^+$  species ( $n = 13, 14$ ) play in planar hypercoordination chemistry has largely omitted in previous investigations and their accurate geometrical and electronic structures and detailed La-C coordination bonding patterns remain to be fully evaluated using the state-of-the-art theoretical approaches to interpret their behaviors observed in experiments.

Detailed first-principles theory calculations performed in this work indicate that the experimentally observed  $\text{La@C}_{13}^+$  (1) with a perfect  $D_{13h}$  symmetry and slightly off-centered  $\text{La@C}_{14}^+$  (4) with a  $C_{2v}$  geometry achieve the record coordination numbers of CN = 13 and 11 in planar species reported to date. The enhanced stability of  $\text{La@C}_{13}^+$  (1) originates from its  $\sigma + \pi$  dual aromaticity with 14 delocalized  $\sigma$  electrons and 14 delocalized  $\pi$  electrons (14  $\sigma + 14 \pi$ ) each matching the  $4N + 2$  aromatic rule ( $N_\sigma = N_\pi = 3$ ).  $\sigma + \pi$  dually aromatic  $D_{13h}$   $\text{Ca@C}_{13}$  (2),  $\text{C}_{13v}$   $\text{Ac@C}_{13}^+$  (3),  $C_{2v}$   $\text{Y@B}_6\text{C}_6^+$  (5), and  $C_{2v}$   $\text{Sc@B}_5\text{C}_6$  (6) have also been obtained at first-principles theory level with CN = 13, 13, 12, and 11, respectively. The highly stable  $\text{La@C}_{13}^+$  (1) is found to behave like a super-hydrogen monocation ( $\text{H}^+$ ) in its substituted complex compounds.

## 2. Theoretical procedure

Extensive global-minimum (GM) searches were performed on  $\text{LaC}_{13}^+$ ,  $\text{LaC}_{14}^+$ ,  $\text{CaC}_{13}$ ,  $\text{AcC}_{13}^+$ ,  $\text{YB}_6\text{C}_6^+$ ,  $\text{ScB}_5\text{C}_6$ , and  $\text{CeC}_{13}^{+/2+}$  using the TGmin2 code<sup>18</sup> at DFT level based on the constraint basin-hopping algorithm.<sup>19</sup> In total, more than 1000 stationary points with different spin multiplicities were probed for each species at PBE/DZVP level using the CP2K program.<sup>20,21</sup> Low-lying isomers were then fully optimized at the M06-2X and PBE0 level,<sup>22,23</sup> with the 6-311+G(d,p) basis sets for C, B, N, Ca, and Sc<sup>24</sup> and Stuttgart relativistic small-core pseudopotentials for La, Y, Ce, and Ac,<sup>25,26</sup> using the Gaussian-16 program suite.<sup>27</sup> Frequency analyses were performed to make sure all the optimized structures are true minima of the systems. Relative energies for the five lowest-lying isomers were further refined using the more accurate coupled cluster method with triple excitations CCSD(T)<sup>28–30</sup> implemented in Molpro<sup>31</sup> with the basis set of cc-pVTZ for C, B, N, Ca, and Sc and the Stuttgart small-core pseudopotential for La, Y, and Ac. The optimized GM structures are summarized in Fig. 1 and more alternative isomers tabulated in Fig. S1–S6.† Natural bonding orbital (NBO) analyses were performed using the NBO 6.0 program.<sup>32</sup> Born–Oppenheimer molecular dynamics (BOMD) simulations were performed on  $\text{LaC}_{13}^+$  (1) for 30 ps using the CP2K software suite

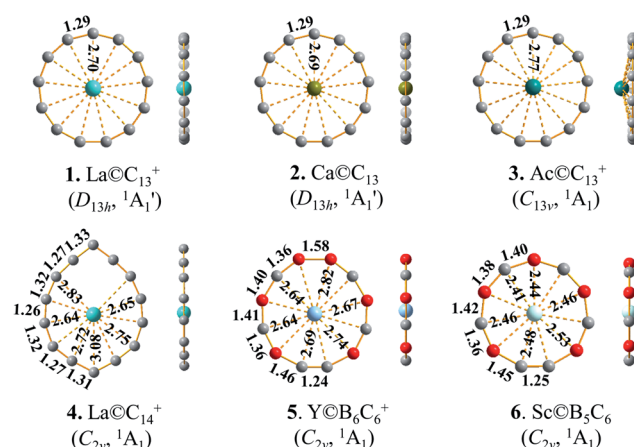


Fig. 1 Top and side views of the optimized  $\text{La@C}_{13}^+$  (1),  $\text{Ca@C}_{13}$  (2),  $\text{Ac@C}_{13}^+$  (3),  $\text{La@C}_{14}^+$  (4),  $\text{Y@B}_6\text{C}_6^+$  (5), and  $\text{Sc@B}_5\text{C}_6$  (6) at M06-2X level, with bond lengths indicated in Å.

at 300, 800, and 1000 K.<sup>21</sup> The anisotropy of the current-induced density (ACID)<sup>33</sup> analyses were performed using the ACID code, with the ring-current maps generated using POV-Ray 3.7.<sup>34</sup> The iso-chemical shielding surfaces (ICSSs)<sup>35,36</sup> were generated with the Multiwfn 3.8 code.<sup>37</sup> The UV-vis spectra were simulated using the time-dependent TD-DFT-M06-2X approach.<sup>38</sup>

## 3. Results and discussion

We start from  $\text{LaC}_{13}^+$ , the most concerned species observed in  $\text{LaC}_n^+$  series ( $n = 12\text{--}40$ ).<sup>13</sup> Encouragingly and interestingly, as shown in Fig. 1 and S1,† extensive GM searches indicate that  $\text{LaC}_{13}^+$  possesses the well-defined perfect planar GM of  $D_{13h}$   $\text{La@C}_{13}^+$  (1) which contains a La atom located exactly at the center of the  $\text{C}_{13}$  wheel ligand, with the optimized La–C coordination bond lengths of  $r_{\text{La-C}} = 2.70$  Å which are slightly longer than the sum of the self-consistent single-bond covalent radii of La and C (2.55 Å)<sup>12</sup> and C–C bond lengths of  $r_{\text{C-C}} = 1.29$  Å which lie between C=C double-bond (1.34 Å) and C≡C triple bond (1.20 Å), setting up the highest coordination number of CN = 13 in planar species reported to date.  $\text{La@C}_{13}^+$  (1) possesses the huge HOMO–LUMO gap of  $\Delta E_{\text{gap}} = 5.33$  eV at M06-2X level, well underlying its high chemical stability. The slightly distorted triplet  $C_s$   $\text{LaC}_{13}^+$  ( $^3A'$ ) appears to be the second lowest-lying isomer lying 2.41 eV above the GM at CCSD(T). The seventh  $C_{2v}$  isomer with a La inserted into the  $\text{C}_{13}$  ring and the fifth  $C_{2v}$  isomer with a La attached to the outside of the  $\text{C}_{13}$  ring are found to lie 3.36 eV and 3.09 eV higher in energy than the GM at M06-2X, respectively. Extensive BOMD simulations indicate that  $\text{La@C}_{13}^+$  (1) is highly dynamically stable at both 800 K and 1000 K, with the small average root-mean-square-deviations of RMSD = 0.11 and 0.13 Å and maximum bond length deviations of MAXD = 0.31 and 0.36 Å, respectively (Fig. S7†). No high-lying isomers were observed during the dynamical simulations.

Replacing the La center in  $\text{La@C}_{13}^+$  (1) with a Ca atom generates the charge-transfer neutral complex  $D_{13h}$   $\text{Ca@C}_{13}$  (2). The Ca center in  $\text{Ca@C}_{13}$  (2) matches the  $\text{C}_{13}$  wheel ligand



perfectly both electronically and geometrically though it has a much lower Wiberg bond index of  $\text{WBI}_{\text{Ca}} = 0.26$  than La in  $\text{La}@\text{C}_{13}^+$  (1) where  $\text{WBI}_{\text{La}} = 1.76$  (Table 1). The Ca–C coordination interaction with the low bond order of  $\text{WBI}_{\text{Ca-C}} = 0.02$  in  $\text{Ca}^{2+}@\text{C}_{13}^{2-}$  (2) is thus almost purely ionic. Using an Ac atom which has a larger atomic radius than La to replace La in  $\text{La}@\text{C}_{13}^+$  (1), the slightly buckled  $\text{C}_{13\text{v}} \text{Ac}@\text{C}_{13}^+$  (3) is generated in which the Ac atom lies 0.59 Å above the  $\text{C}_{13}$  ring, with the periphery C–C distances of  $r_{\text{C-C}} = 1.29$  Å remaining basically unchanged. The experimentally observed prominent  $\text{ScC}_{13}^+$  and  $\text{YC}_{13}^+$  monocations<sup>15</sup> have severely off-centered  $\text{C}_{2\text{v}} \text{Sc}@\text{C}_{13}^+$  ( $^1\text{A}_1$ ) (with CN = 8) and  $\text{C}_{2\text{v}} \text{Y}@\text{C}_{13}^+$  ( $^1\text{A}_1$ ) (with CN = 9) GM structures due to strong ring strains, respectively, while the open-shell  $\text{CeC}_{13}^+$  possesses a slightly distorted GM  $\text{C}_{2\text{v}} \text{Ce}@\text{C}_{13}^+$  ( $^2\text{B}_2$ ) which has practically a  $D_{13\text{h}}$  symmetry (Fig. S8†). With one more valence electron detached, the  $\text{Ce}@\text{C}_{13}^{2+}$  dication isovalent with  $\text{La}@\text{C}_{13}^+$  (1) has indeed a perfect  $D_{13\text{h}}$  GM (Fig. S8†).

It is natural to ask at current stage whether it is possible to form metal-centered monocyclic carbon wheel clusters with coordination numbers greater than thirteen (*i.e.*,  $\text{CN} > 13$ ). We carefully checked the hypercoordination chemistry of the experimentally observed  $\text{La}@\text{C}_{14}^+$  in this work. Although a bare  $\text{C}_{14}$  has a perfect  $\text{C}_{7\text{h}}$  acetylenic structure,<sup>39</sup> with a La atom added in, the La-doped  $\text{LaC}_{14}^+$  possesses the off-centered planar GM of  $\text{C}_{2\text{v}} \text{La}@\text{C}_{14}^+$  (4) which has the actual coordination number of CN = 11 (Fig. 1 and S4†). The three C atoms on the top part of  $\text{La}@\text{C}_{14}^+$  (4) with La–C distances great than 3.1 Å have the practically negligible La–C coordination bond orders (with  $\text{WBI}_{\text{La-C}} \approx 0.00$ ). Using Ac, the largest actinide metal in the periodical table, to replace La,<sup>12</sup> an elongated planar  $D_{2\text{h}} \text{Ac}@\text{C}_{14}^+$  (Fig. S8†) with CN = 12 is generated. A  $\text{C}_{14}$  ring is obviously too big in size to host a transition-metal atom at its geometrical center comfortably to form a perfect wheel complex  $D_{nh} \text{M}@\text{C}_n$  with the same M–C coordination bonding distances. We conclude that CN = 13 is the highest coordination number in metal-centered monocyclic carbon wheel clusters  $\text{M}@\text{C}_n^+$  with effective M–C coordination interactions.

Introducing certain numbers of B atoms into the carbon rings generates more structural diversities in B–C binary wheel ligands  $\text{B}_m\text{C}_n$  with  $\text{CN} \leq 13$ . As examples, the metal-centered

monocyclic C–B binary wheel complexes  $\text{Y}@\text{B}_6\text{C}_6^+$  (5) and  $\text{Sc}@\text{B}_5\text{C}_6$  (6) in Fig. 1 and  $\text{C}_{2\text{v}} \text{La}@\text{BC}_{12}$  in Fig. S8† as the GMs of the systems possess the coordination numbers of CN = 12, 11, and 13, respectively. These planar C–B binary wheel complexes have larger C–B and B–B periphery distances than the corresponding C–C distances in  $\text{La}@\text{C}_{13}^+$  (1) because B has a larger covalent radius than C.

To interpret the high stabilities of these hypercoordinated planar species, we performed detailed NBO and molecular orbital analyses on  $\text{La}@\text{C}_{13}^+$  (1),  $\text{Y}@\text{B}_6\text{C}_6^+$  (5), and  $\text{Sc}@\text{B}_5\text{C}_6$  (6). As tabulated in Table 1, the La center in  $\text{La}@\text{C}_{13}^+$  (1) possesses the natural atomic charge of  $q_{\text{La}} = +2.08$  |e|, electronic configuration of  $\text{La}[\text{Xe}]4\text{f}^{0.43}5\text{d}^{0.41}6\text{s}^{0.02}$ , and total Wiberg bond order of  $\text{WBI}_{\text{La}} = 1.76$ . The C atoms on the  $\text{C}_{13}$  wheel ligand have the total Wiberg bond orders of  $\text{WBI}_{\text{C}} = 3.99$  and C–C bond orders of  $\text{WBI}_{\text{C-C}} = 1.73$ , revealing the cumulenenic nature of the complex. Obviously, the La center donates its 6s electron almost completely to the  $\text{C}_{13}$  ligand. The La– $\text{C}_{13}$  coordination

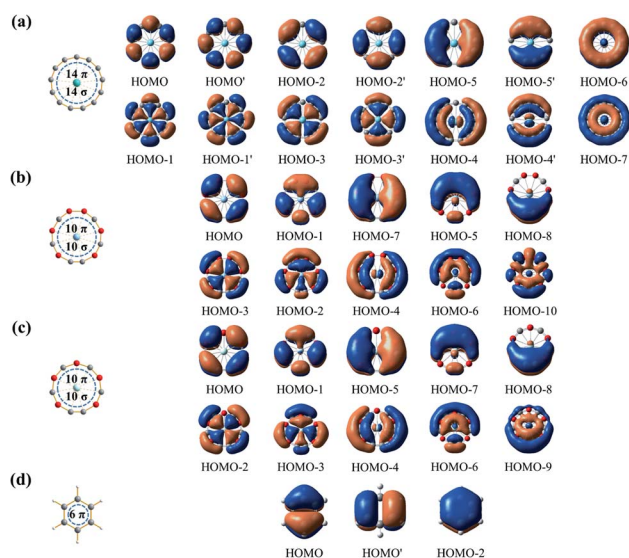


Fig. 2 Delocalized  $\pi$ - and  $\sigma$ -CMOs of (a)  $\text{La}@\text{C}_{13}^+$  (1), (b)  $\text{Y}@\text{B}_6\text{C}_6^+$  (5), and (c)  $\text{Sc}@\text{B}_5\text{C}_6$  (6), in comparison with the delocalized  $\pi$ -CMOs of (d)  $D_{6\text{h}} \text{C}_6\text{H}_6$ .

**Table 1** Calculated HOMO–LUMO gaps  $\Delta E_{\text{gap}}$ /eV, natural atomic charges  $q_{\text{M}}$ , electronic configurations, and Wiberg bond indexes  $\text{WBI}_{\text{M}}$  of the metal centers M and Wiberg bond indexes of the M–C ( $\text{WBI}_{\text{M-C}}$ ) and M–B ( $\text{WBI}_{\text{M-B}}$ ) coordination interactions and NICS values 1.0 Å above the metal centers (NICS (1)) of the  $\text{M}^{(x)}@\text{B}_m\text{C}_n^{k\pm}$  complex series (1–6) at M06-2X level

$\text{M}^{(x)}@\text{B}_m\text{C}_n^{k\pm}$	CN	$\Delta E_{\text{gap}}$ /eV	$q_{\text{M}}$	Electronic configurations of central metal M	$\text{WBI}_{\text{M}}$	$\text{WBI}_{\text{M-C}}$	$\text{WBI}_{\text{M-B}}$	NICS (1)
$D_{13\text{h}} \text{La}@\text{C}_{13}^+$ (1)	13	5.33	2.08	$[\text{Xe}] 4\text{f}^{0.43}5\text{d}^{0.41}6\text{s}^{0.02}$	1.76	0.14	—	−58.54
$D_{13\text{h}} \text{Ca}@\text{C}_{13}$ (2)	13	5.63	1.87	$[\text{Ar}] 3\text{d}^{0.09}4\text{s}^{0.03}4\text{p}^{0.01}$	0.26	0.02	—	−44.68
$\text{C}_{13\text{v}} \text{Ac}@\text{C}_{13}^+$ (3)	13	5.26	2.38	$[\text{Rn}] 5\text{f}^{0.19}6\text{d}^{0.35}7\text{s}^{0.03}$	1.22	0.10	—	−55.16
$\text{C}_{2\text{v}} \text{La}@\text{C}_{14}^+$ (4)	11	3.72	2.15	$[\text{Xe}] 4\text{f}^{0.28}5\text{d}^{0.50}6\text{s}^{0.03}$	1.64	0.07–0.16	—	−29.21
$\text{C}_{2\text{v}} \text{Y}@\text{B}_6\text{C}_6^+$ (5)	12	5.70	2.12	$[\text{Kr}] 5\text{s}^{0.06}4\text{d}^{0.70}5\text{p}^{0.01}$	1.67	0.10–0.22	0.09–0.12	−24.08
$\text{C}_{2\text{v}} \text{Sc}@\text{B}_5\text{C}_6$ (6)	11	5.32	1.94	$[\text{Ar}] 3\text{d}^{0.87}4\text{s}^{0.07}4\text{p}^{0.02}$	1.94	0.13–0.29	0.13–0.14	−29.62



interactions mainly originate from contributions involving the 5d and 4f atomic orbitals of the La center, as indicated in the degenerated  $\pi$ -HOMO/HOMO',  $\pi$ -HOMO-2/HOMO-2',  $\sigma$ -HOMO-1/HOMO-1', and  $\sigma$ -HOMO-3/HOMO-3 in Fig. 2(a). Although each La–C coordination interaction in  $\text{La@C}_{13}^+$  (**1**) has a relatively low bond order ( $\text{WBI}_{\text{La-C}} = 0.14$ ), the thirteen equivalent La–C coordination bonds function together to effectively stabilize the hypercoordinated cluster, making it the well-defined GM of the system observed solely in gas-phase experiments.<sup>13,14</sup> Similar situations happen in  $\text{Ac@C}_{13}^+$  (**3**),  $\text{Y@B}_6\text{C}_6^+$  (**5**), and  $\text{Sc@B}_5\text{C}_6$  (**6**).

The 14 totally delocalized canonical molecular orbitals (CMOs) of  $\text{La@C}_{13}^+$  (**1**) are collectively shown in Fig. 2(a), including 7 delocalized  $\pi$ -CMOs and 7 delocalized  $\sigma$ -CMOs. Its remaining 13  $\sigma$ -CMOs correspond to 13 two-center-two-electron (2c-2e) C–C  $\sigma$  bonds along the periphery of the  $\text{C}_{13}$  ligand (Fig. S9†). The degenerate f-type HOMO/HOMO', d-type HOMO-2/HOMO-2' and p-type HOMO-5/HOMO-5' and non-degenerate s-type HOMO-6 possess three, two, one, and zero nodal surfaces, respectively, forming an out-of-plane 14  $\pi$  electron system matching the  $4N_\pi + 2$  aromatic rule with  $N_\pi = 3$ . Similarly, the degenerate HOMO-1/HOMO-1', HOMO-3/HOMO-3', and HOMO-4/HOMO-4' and non-degenerate HOMO-7 form an in-plane 14  $\sigma$  electron system matching the  $4N_\sigma + 2$  aromatic rule with  $N_\sigma = 3$ . Such a unique 14  $\sigma + 14 \pi$  electronic configuration renders  $\sigma + \pi$  dual aromaticity to  $\text{La@C}_{13}^+$  (**1**), effectively stabilizing the monocation observed in experiments, similar to the situation in the  $\sigma + \pi$  dually aromatic  $D_{10h}$   $\text{Ta@B}_{10}^-$  which possesses a 10  $\sigma + 6 \pi$  electronic configuration.<sup>1</sup> It is noticed that metal-centered wheel  $D_{13h}$   $\text{La@C}_{13}^+$  (**1**) has the same numbers of delocalized  $\sigma$  and  $\pi$  electrons (14  $\sigma + 14 \pi$ ) as the highly stable ring-like acetylenic  $\text{C}_{7h}$   $\text{C}_{14}$ .<sup>39</sup>

As shown in Fig. 2(b) and (c), both the metal-centered monocyclic C–B binary wheel clusters  $\text{Y@B}_6\text{C}_6^+$  (**5**) and  $\text{Sc@B}_5\text{C}_6$  (**6**) have 5 delocalized  $\pi$ -CMOs and 5 delocalized  $\sigma$ -CMOs, forming an out-of-plane 10  $\pi$  electron system conforming to the  $4N_\pi + 2$   $\pi$ -aromatic rule ( $N_\pi = 2$ ) and an in-plane 10  $\sigma$  electron system conforming to  $4N_\sigma + 2$   $\sigma$  aromatic rule ( $N_\sigma = 2$ ). Such 10  $\sigma + 10 \pi$  electronic configurations make both  $\text{Y@B}_6\text{C}_6^+$  (**5**) and  $\text{Sc@B}_5\text{C}_6$  (**6**)  $\sigma + \pi$  dually aromatic in nature, similar to but with more delocalized electrons than the previously reported  $\text{Co@B}_8^-$  and  $\text{Ru@B}_9^-$  with 6  $\sigma + 6 \pi$  delocalized electrons and  $\text{Ta@B}_{10}^-$  and  $\text{Nb@B}_{10}^-$  with 10  $\sigma + 6 \pi$  delocalized electrons.<sup>1,5–8</sup>

The La– $\text{C}_{13}$  coordination interactions in  $\text{La@C}_{13}^+$  (**1**) mainly originate from d–p and f–p  $\sigma$ -coordination interactions involving the in-plane La  $5d_{x^2-y^2}/5d_{xy}$  and  $4f_{x(x^2-3y^2)}/4f_{y(y^2-3x^2)}$  atomic orbitals and C  $2p_x/2p_y$  hybridized atomic orbitals, as demonstrated in the degenerated HOMO-3/HOMO-3' (5d–2p  $\sigma$ -coordination) and HOMO-1/HOMO-1' (4f–2p  $\sigma$ -coordination) in Fig. 2(a), respectively. Quantitatively, the La center contributes more to the delocalized in-plane  $\sigma$ -CMOs (2.81–7.63%) than to the delocalized out-of-plane  $\pi$ -CMOs (0.08–3.66%). The delocalized in-plane  $\sigma$ -CMOs thus dominate the La–C coordination bonding interactions. Similarly, the in-plane 4d–2p  $\sigma$ -coordination interactions (HOMO-2 and HOMO-3) in  $\text{Y@B}_6\text{C}_6^+$  (**5**) and 3d–2p  $\sigma$ -coordination interactions (HOMO-2 and HOMO-3) in

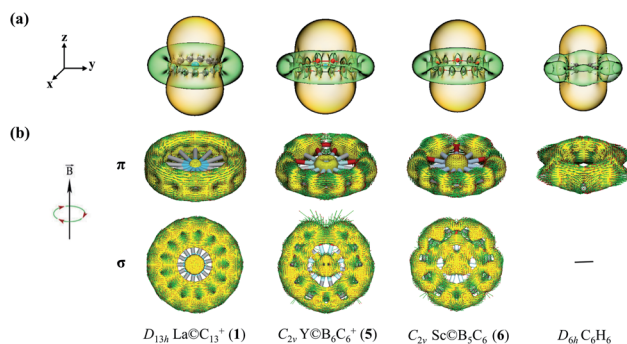


Fig. 3 (a) Calculated iso-chemical shielding surfaces (ICSSs) of  $\text{La@C}_{13}^+$  (**1**),  $\text{Y@B}_6\text{C}_6^+$  (**5**), and  $\text{Sc@B}_5\text{C}_6$  (**6**), compared with that of aromatic benzene  $\text{C}_6\text{H}_6$ . Yellow and green regions stand for chemical shielding and de-shielding areas, respectively. (b) Calculated  $\pi$ - and  $\sigma$ -ring current maps of  $\text{La@C}_{13}^+$  (**1**),  $\text{Y@B}_6\text{C}_6^+$  (**5**), and  $\text{Sc@B}_5\text{C}_6$  (**6**), respectively, in comparison with the  $\pi$ -ring current map of  $\text{D}_{6h}$   $\text{C}_6\text{H}_6$ . The external magnetic field is perpendicular to the wheel plane. The red arrows represent directions and magnitudes of the ring currents at various positions on the ACID iso-surfaces.

$\text{Sc@B}_5\text{C}_6$  (**6**) dominate the metal–ligand interactions in the two 10  $\sigma + 10 \pi$  systems.

The aromatic nature of  $\text{La@C}_{13}^+$  (**1**),  $\text{Y@B}_6\text{C}_6^+$  (**5**), and  $\text{Sc@B}_5\text{C}_6$  (**6**) is further evidenced by their calculated nucleus-independent chemical shift (NICS) values. Based on the calculated NICS-ZZ components, Fig. 3(a) depicts the ICSS surfaces of **1**, **5**, and **6** with the Z-axis perpendicular to the molecular planes to illuminate the chemical shielding around the metal centers, in comparison with that of the prototypical aromatic benzene ( $\text{C}_6\text{H}_6$ ). Obviously, the space inside the  $\text{C}_{13}$ ,  $\text{B}_6\text{C}_6$ , or  $\text{B}_5\text{C}_6$  rings in horizontal direction or within about 1.0 Å above the metal centers in vertical direction belong to chemical shielding regions with negative NICS-ZZ values (highlighted in yellow), while the chemical de-shielding areas with positive NICS values (highlighted in green) are located outside the wheel ligands in horizontal direction. Fig. 3(a) clearly shows the ICSS surfaces of these metal-centered planar complexes are exactly similar to that of the aromatic benzene.

Calculating the anisotropy of current-induced density (ACID)<sup>34</sup> is an effective approach to graphically display the ring currents induced by an external magnetic field in vertical directions perpendicular to the molecular planes. ACID can be decomposed into  $\sigma$  and  $\pi$  components separately. Fig. 3(b) clearly indicates the  $\pi$ -ring current maps of  $\text{La@C}_{13}^+$  (**1**),  $\text{Y@B}_6\text{C}_6^+$  (**5**), and  $\text{Sc@B}_5\text{C}_6$  (**6**) are extremely similar to the corresponding  $\pi$ -ring current map of  $\pi$ -aromatic benzene  $\text{C}_6\text{H}_6$ . Besides, in contrast to benzene which possesses no delocalized  $\sigma$ -electrons,  $\text{La@C}_{13}^+$  (**1**),  $\text{Y@B}_6\text{C}_6^+$  (**5**), and  $\text{Sc@B}_5\text{C}_6$  (**6**) also exhibit strong  $\sigma$ -ring currents, rendering additional  $\sigma$ -aromaticity to stabilize the systems, as shown in Fig. 3(b) (see Fig. S10† for high-resolution  $\pi$ - and  $\sigma$ -ring current maps of **1**, **5**, and **6**). The observation of both  $\sigma$ - and  $\pi$ -diatropic ring currents in **1**, **5**, and **6** well supports the  $\sigma + \pi$  dually aromatic nature of these planar hypercoordinated complexes.

Based on the planar hypercoordinated species discussed above, we develop a universal electronic design principle for  $\sigma +$



$\pi$  dually aromatic metal-centered monocyclic boron, carbon, or boron-carbon binary wheel clusters  $M^{(x)}@B_mC_n^{k\pm}$ . There exist  $m + n$   $2c-2e$   $\sigma$  bonds along the periphery of the monocyclic  $B_mC_n$  wheel ligand. With each C atom providing two delocalized electrons and each B atom contributing one delocalized electron, the total number of the delocalized electrons in  $M^{(x)}@B_mC_n^{k\pm}$  matches the requirement of  $\sigma + \pi$  dual aromaticity of the system:

$$m + 2n + x \pm k = L \quad (L = 12, 16, 20, \text{ or } 28) \quad (1)$$

where  $L$  is the total number of delocalized  $\sigma$  and  $\pi$  electrons each matching the  $4N + 2$  rule and  $x$  stands for the formal valence of the central atom  $M$ . Such an electronic design principle covers the previously observed  $D_{7h}$   $B@B_7^{2-}$ ,  $D_{8h}$   $B@B_8^-$ ,  $D_{9h}$   $Co@B_8^-$ , and  $D_{9h}$   $Ru@B_9^-$  where  $L = 12$  and  $x = 3, 3, 3$ , and  $2$  and  $D_{10h}$   $Ta@B_{10}^-$  and  $D_{10h}$   $Nb@B_{10}^-$  where  $L = 16$  and  $x = 5$  and  $5$ , respectively. For the currently discussed  $La@C_{13}^+$  (1),  $Ca@C_{13}$  (2), and  $Ac@C_{13}^+$  (3),  $L = 28$  and  $x = 3, 2$ , and  $3$ , while for  $Y@B_6C_6^+$  (5) and  $Sc@B_5C_6$  (6),  $L = 20$  and  $x = 3$  and  $3$ , respectively. The slightly buckled  $C_{13v}$   $Ac@C_{13}^+$  (3) follows the same electronic design principle though the Ac center in it slightly mismatches the  $C_{13}$  wheel ligand in geometry. Eqn (1) can be easily extended to  $\sigma + \pi$  dually aromatic B–C–N ternary wheel complexes  $M^{(x)}@B_mC_nN_l^{k\pm}$  where it reads:  $m + 2n + 3l + x \pm k = 28$ , as demonstrated in the cases of  $C_s$   $La@BNC_{11}^+$  and  $C_s$   $La@B_4N_4C_5^+$  (Fig. S8†) in which each N atom contributes three valence electrons to the delocalized systems. However, extensive test calculations indicate that inclusion B or N atoms in the wheel ligands does not help to improve the maximum coordination numbers of the systems.

The highly stable  $La@C_{13}^+$  (1) with a wide HOMO–LUMO gap and fully occupied bonding inner-shell CMOs can be used as a super-hydrogen monocation ( $H^+$ ) to form various substituted multi-nuclei complexes. Typical examples include  $C_{13v}$   $[La@C_{13}]X$  ( $X = F, Cl, Br$ ) (7),  $D_{13h}$   $[La@C_{13}]^+L_2$  ( $L = Ar, Kr$ ) (8),  $C_{2v}$   $[La@C_{13}]_2O$  (9), and  $C_{3v}$   $N[La@C_{13}]_3$  (10) (Fig. 4) which can be derived from the parent species  $C_{\infty v}$   $HX$ ,  $D_{\infty h}$   $H^+L_2$ ,  $C_{2v}$   $H_2O$ , and  $C_{3v}$   $NH_3$  by substituting  $H^+$  monocation(s) with  $La@C_{13}^+$  (1) unit(s), respectively, presenting the viable possibility to form complex compounds with multiple hypercoordinated metal centers.

Finally, as examples, the simulated IR, Raman, and UV-vis spectra of  $D_{13h}$   $La@C_{13}^+$  (1) and  $C_{2v}$   $Y@B_6C_6^+$  (5) are presented in Fig. S11† to facilitate their spectroscopic characterizations.  $La@C_{13}^+$  (1) possesses highly simplified spectra due to its perfect  $D_{13h}$  symmetry. It has two main IR peaks at  $39$  ( $a_2''$ ) and

$866$  ( $e_1'$ )  $cm^{-1}$ , three Raman peaks at  $272$  ( $e_2'$ ),  $664$  ( $a_1'$ ), and  $1280$  ( $e_2'$ )  $cm^{-1}$ , and three UV absorption peaks at  $156$  ( $A_1'$ ),  $174$  ( $E_2'$ ), and  $200$  ( $E_2'$ ) nm, respectively.  $C_{2v}$   $Y@B_6C_6^+$  (5) has more complicated spectra, with two main IR absorption peaks at  $499$  ( $b_1$ ) and  $588$  ( $b_2$ )  $cm^{-1}$ , two major Raman scattering bands at  $211$  ( $b_2$ ) and  $623$  ( $a_1$ )  $cm^{-1}$ , and five UV absorption bands around  $134$  ( $^1B_2$ ),  $161$  ( $^1A_1$ ),  $191$  ( $^1B_2$ ),  $207$  ( $^1A_1$ ), and  $219$  ( $^1B_2$ ) nm, respectively.

## 4. Conclusions

Extensive first-principles theory calculations performed in this work unveil the highest coordination numbers of CN = 13 in  $La@C_{13}^+$  (1),  $Ca@C_{13}$  (2), and  $Ac@C_{13}^+$  (3), CN = 12 in  $Y@B_6C_6^+$  (5), and CN = 11 in  $La@C_{14}^+$  (4) and  $Sc@B_5C_6$  (6) reported to date in planar species, effectively enriching the structural and bonding patterns in planar hypercoordination chemistry.  $\sigma + \pi$  dually aromatic metal-centered monocyclic B–C binary wheel complexes  $M^{(x)}@B_mC_n^{k\pm}$  follow the electronic design principle of  $m + 2n + x \pm k = L$  ( $L = 12, 16, 20$ , or  $28$ ) which can be readily extended to more complicated systems containing other periphery atoms rather than B and C. The recent experimental identification of the sp-hybridized molecular carbon allotrope,  $\pi$ -aromatic  $C_{18}$ , induced by atom manipulations,<sup>9</sup> presents the possibility to synthesize and characterize the  $\sigma + \pi$  dually aromatic  $La@C_{13}^+$  (1) and its complex compounds to open a new area in planar hypercoordination chemistry, catalysis, and materials science.

## Conflicts of interest

There are no conflicts to declare.

## Acknowledgements

The work was supported by the National Natural Science Foundation of China (21720102006 and 21973057 to S.-D. Li).

## Notes and references

- 1 T. R. Galeev, C. Romanescu, W. L. Li, L. S. Wang and A. I. Boldyrev, *Angew. Chem., Int. Ed.*, 2012, **51**, 2101–2105.
- 2 T. Heine and G. Merino, *Angew. Chem., Int. Ed.*, 2012, **51**, 4275–4276.
- 3 H. J. Zhai, A. N. Alexandrova, K. A. Birch, A. I. Boldyrev and L. S. Wang, *Angew. Chem., Int. Ed.*, 2003, **42**, 6004–6008.
- 4 C. Romanescu, T. R. Galeev, W. L. Li, A. I. Boldyrev and L. S. Wang, *Angew. Chem., Int. Ed.*, 2011, **123**, 9506–9509.
- 5 C. Romanescu, T. R. Galeev, W. L. Li, A. I. Boldyrev and L. S. Wang, *Angew. Chem., Int. Ed.*, 2011, **50**, 9334–9337.
- 6 C. Romanescu, T. R. Galeev, W. L. Li, A. I. Boldyrev and L. S. Wang, *Acc. Chem. Res.*, 2013, **46**, 350–358.
- 7 C. Romanescu, T. R. Galeev, W. L. Li, A. I. Boldyrev and L. S. Wang, *J. Chem. Phys.*, 2013, **138**, 134315.
- 8 W. L. Li, C. Romanescu, T. R. Galeev, Z. A. Piazza, A. I. Boldyrev and L. S. Wang, *J. Am. Chem. Soc.*, 2012, **134**, 165–168.

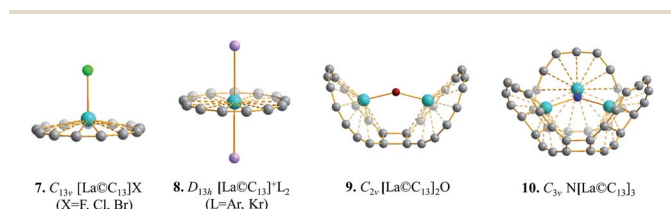


Fig. 4 Optimized structures of  $[La@C_{13}]X$  (7) ( $X = F, Cl, Br$ ),  $[La@C_{13}]^+L_2$  (8) ( $L = Ar, Kr$ ),  $[La@C_{13}]_2O$  (9), and  $N[La@C_{13}]_3$  (10) at M06-2X level.



- 9 K. Kaiser, L. M. Scriven, F. Schulz, P. Gawel, L. Gross and H. L. Anderson, *Science*, 2019, **365**, 1299–1301.
- 10 Z. Liu, X. Wang, T. Lu, A. Yuan and X. Yan, *ChemRxiv*, 2021, DOI: 10.26434/chemrxiv.14601168.v1.
- 11 Y. Jiang, Y. Wu, J. Deng and Z. Wang, *Phys. Chem. Chem. Phys.*, 2021, **23**, 8817–8824.
- 12 P. Pykkö and M. Atsumi, *Chem.–Eur. J.*, 2009, **15**, 12770–12779.
- 13 D. E. Clemmer, K. B. Shelimov and M. F. Jarrold, *J. Am. Chem. Soc.*, 1994, **116**, 5971–5972.
- 14 K. B. Shelimov, D. E. Clemmer and M. F. Jarrold, *J. Phys. Chem.*, 1995, **99**, 11376–11386.
- 15 R. Klingeler, P. S. Bechthold, M. Neeb and W. Eberhardt, *J. Chem. Phys.*, 2000, **113**, 4.
- 16 S. Roszak and K. Balasubramanian, *Chem. Phys. Lett.*, 1997, **264**, 80–84.
- 17 D. L. Strout and M. B. Hall, *J. Phys. Chem. A*, 1998, **102**, 641–645.
- 18 X. Chen, Y. F. Zhao, Y. Y. Zhang and J. Li, *J. Comput. Chem.*, 2019, **40**, 1105–1112.
- 19 D. J. Wales and H. A. Scheraga, *Science*, 1999, **285**, 1368–1372.
- 20 J. P. Perdew, K. Burke and M. Ernzerhof, *Phys. Rev. Lett.*, 1996, **77**, 3865.
- 21 J. VandeVondele, M. Krack, F. Mohamed, M. Parrinello, T. Chassaing and J. Hutter, *Comput. Phys. Commun.*, 2005, **167**, 103–128.
- 22 Y. Zhao and D. G. Truhlar, *Theor. Chem. Acc.*, 2008, **120**, 215–241.
- 23 C. Adamo and V. Barone, *J. Chem. Phys.*, 1999, **110**, 6158–6170.
- 24 R. Krishnan, J. S. Binkley, R. Seeger and J. A. Pople, *J. Chem. Phys.*, 1980, **72**, 650–654.
- 25 D. Feller, *J. Comput. Chem.*, 1996, **17**, 1571–1586.
- 26 L. Schuchardt, B. T. Didier, T. Elsethagen, L. Sun, V. Gurumoorthi, J. Chase, J. Li and T. L. Windus, *J. Chem. Inf. Model.*, 2007, **47**, 1045–1052.
- 27 M. J. Frisch, *et al.*, *Gaussian 16, Revision A.03*, Gaussian Inc., Wallingford, CT, 2016.
- 28 J. Čížek, *Adv. Chem. Phys.*, 1969, **14**, 35.
- 29 G. D. Purvis III and R. J. Bartlett, *J. Chem. Phys.*, 1982, **76**, 1910.
- 30 K. Raghavachari, G. W. Trucks, J. A. Pople and M. Head-Gordon, *Chem. Phys. Lett.*, 1989, **157**, 479–483.
- 31 H. J. Werner, *et al.*, *Molpro, version.1.*, 2012, ([www.molpro.net](http://www.molpro.net)).
- 32 P. E. D. Glendening, J. K. Badenhoop, A. E. Reed, J. E. Carpenter, J. A. Bohmann, C. M. Morales, C. R. Landis and F. Weinhold, *NBO 6.0*, 2013.
- 33 D. Geuenich, K. Hess, F. Köhler and R. Herges, *Chem. Rev.*, 2005, **105**, 3758–3772.
- 34 Povray, Persistence of vision raytracer, *POV-Ray 3.7*, <http://www.povray.org>.
- 35 S. Klod and E. Kleinpeter, *J. Chem. Soc., Perkin Trans. 2*, 2001, **2**, 1893–1898.
- 36 E. Kleinpeter, S. Klod and A. Koch, *J. Mol. Struct.*, 2007, **811**, 45–60.
- 37 T. Lu and F. W. Chen, *J. Comput. Chem.*, 2012, **33**, 580–592.
- 38 R. Bauernschmitt and R. Ahlrichs, *Chem. Phys. Lett.*, 1996, **256**, 454–464.
- 39 S. Arulmozhiraja and T. Ohno, *J. Chem. Phys.*, 2008, **128**, 114301.

